Ising-like anisotropy stabilized $\frac{1}{3}$ and $\frac{2}{3}$ magnetization plateaus in the V^{3+} kagome lattice antiferromagnets $Cs_2KV_3F_{12}$, $Cs_2NaV_3F_{12}$, and $Rb_2NaV_3F_{12}$

Masato Goto,[1,*] Hiroaki Ueda,[1] Chishiro Michioka,[1] Akira Matsuo,[2] Koichi Kindo,[2] Kento Sugawara,[3] Shintaro Kobayashi,[3] Naoyuki Katayama,[3] Hiroshi Sawa,[3] and Kazuyoshi Yoshimura[1,4,†]

[1]*Department of Chemistry, Graduate School of Science, Kyoto University, Kyoto 606-8502, Japan*

[2]*Institute for Solid State Physics, The University of Tokyo, Kashiwanoha, Kashiwa, Chiba 277-8581, Japan*

[3]*Department of Applied Physics, Graduate School of Engineering, Nagoya University, Aichi 464-8603, Japan*

[4]*Research Center for Low Temperature and Materials Sciences, Kyoto University, Kyoto 606-8502, Japan*

(Received 7 December 2016; revised manuscript received 1 April 2017; published 20 April 2017)

We have investigated crystal structure and magnetic properties of three $S = 1$ V^{3+} Ising-like anisotropic kagome lattice antiferromagnets, $Cs_2KV_3F_{12}$, $Cs_2NaV_3F_{12}$, and $Rb_2NaV_3F_{12}$, using single crystals. Each compound crystallizes in a monoclinic system and has a slightly distorted kagome lattice. Although the magnetic properties are similar, the details depend on the magnitude of magnetic anisotropy. The magnetization and magnetic susceptibility are highly anisotropic owing to anisotropic g factors and Ising-like single ion anisotropy originating from partially unquenched orbital moments of V^{3+}, and the easy axis of Ising-like anisotropy is perpendicular to the kagome plane. In contrast to disordered ground states in the isostructural Ti^{3+} ($S = 1/2$) compounds, the V^{3+} ($S = 1$) compounds exhibit antiferromagnetic ordering with distorted 120° structure or other nearly coplanar magnetic structure whose basal spin plane includes the easy axis, which is mainly due to large magnetic anisotropy and decrease of quantum fluctuation. Moreover, when magnetic fields are applied perpendicular to the kagome plane, magnetization curves of them show distinct 1/3 and 2/3 magnetization plateaus, which are stabilized by Ising-like single ion anisotropy. In particular, the 2/3 magnetization plateaus are notable magnetic phenomena in kagome lattice antiferromagnets and are due to the combination of spin frustration, Ising-like single ion anisotropy, and the small monoclinic distortion of kagome lattices.

DOI: 10.1103/PhysRevB.95.134436

I. INTRODUCTION

Geometrically frustrated antiferromagnets have been of great interest over the past few decades [1]. Among them, kagome lattice antiferromagnets (KLAFs) are known as one of the most fascinating frustrated spin systems and have been intensively studied from the viewpoint of combination of strong quantum fluctuation and spin frustration [2–25]. KLAFs have been expected to show various exotic ground states such as a spin liquid state, which strongly depend on the consisting magnetic ions, quantum fluctuation, magnetic anisotropy, the Dzaloshinsky-Moriya (DM) interaction, and so on. For example, Heisenberg $S = 1/2$ KLAFs have proposed to show a gapped [3–8] or gapless [9–11] spin liquid ground state, whereas a hexagonal [12,13] or trigonal [14,15] valence bond solid state has been proposed as the ground state in the case of $S = 1$. When Ising-like magnetic anisotropy is present in Heisenberg KLAFs, the system was predicted to show a magnetic phase transition at finite temperature [16]. The Dzaloshinsky-Moriya (DM) interaction is known to stabilize the "$q = 0$" 120° structure [17], as is observed in jarosite $KFe_3(OH)_6(SO_4)_2$ [18] and $KCr_3(OH)_6(SO_4)_2$ [19].

Other interesting magnetic phenomena expected in KLAFs are magnetic field induced phase transitions including a 1/3 magnetization plateau. The most intensively studied examples of the 1/3 magnetization-plateau state are triangular lattice antiferromagnets (TLAFs). In TLAFs with Ising-like anisotropy, a 1/3 magnetization-plateau state was predicted to be stabilized when magnetic fields were applied parallel to the easy axis [26]. Moreover, even in the ideal Heisenberg TLAFs with small quantum spin number, a 1/3 magnetization plateau was predicted irrespective of the direction of magnetic fields owing to quantum fluctuation [27]. Indeed, distinct 1/3 magnetization plateaus are experimentally observed under either in-plane or out-plane magnetic fields in some TLAFs, such as large spin system $S = 7/2$ $GdPd_2Al_3$ [28] and $S = 5/2$ $RbFe(MoO_4)_2$ [29], and quantum spin system $J_{\mathrm{eff}} = 1/2$ $Ba_3CoSb_2O_9$ [30]. In particular, in $Ba_3CoSb_2O_9$ with weak easy plane magnetic anisotropy, the magnetization curve under in-plane magnetic fields is in good agreement with theoretical calculations, and quantum fluctuation is considered to be one of the most important driving forces to stabilize the 1/3 magnetization plateau [30].

Similar to TLAFs, KLAFs with Ising-like anisotropy are considered to show a 1/3 magnetization plateau when magnetic fields are applied parallel to the easy axis. Moreover, recently, a 1/3 magnetization plateau has been proposed to appear under high magnetic fields even in the ideal Heisenberg $S = 1/2$–2 KLAFs [20–22]. However, experimentally, there are only a few observations of a 1/3 magnetization plateau irrespective of magnitude of magnetic anisotropy, such as a weak 1/3 magnetization-plateau-like anomaly observed in $S = 3/2$ $KCr_3(OH)_6(SO_4)_2$ [19] for in-plane magnetic fields and $S = 1/2$ $Cs_2BTi_3F_{12}$ (B = K, Na) [23] irrespective of the direction of magnetic fields. In contrast, it was reported that m-N-methylpyridinium nitronylnitroxide (m-MPYNN) · BF_4, which is regarded as $S = 1$ KLAFs at low temperatures [24], shows not a 1/3 magnetization plateau but a 1/2 magnetization-plateau-like step under high magnetic fields [25]. In (m-MPYNN) · BF_4, formation of magnetic

*goto@kuchem.kyoto-u.ac.jp
†kyhv@kuchem.kyoto-u.ac.jp

superstructure was suggested [25]. Hence, in order to reveal the magnetic properties of KLAFs under high magnetic fields, it is needed to experimentally examine magnetic field induced unconventional phenomena including a 1/3 magnetization plateau.

As well as Co^{2+} compounds, V^{3+} compounds tend to be magnetically anisotropic owing to orbital contribution. Hence it is likely that V^{3+} KLAFs exhibit intriguing magnetic phenomena under high magnetic fields. We have reported crystal structure and magnetic properties of $S = 1/2$ Ti^{3+} kagome fluorides $Cs_2KTi_3F_{12}$, $Cs_2NaTi_3F_{12}$, and $Rb_2NaTi_3F_{12}$ [23]. Subsequently, we have discovered three $S = 1$ V^{3+} kagome fluorides $Cs_2KV_3F_{12}$, $Cs_2NaV_3F_{12}$, and $Rb_2NaV_3F_{12}$. By studying these compounds, we can elucidate the effect of magnetic anisotropy on the magnetism of KLAFs. In addition, KLAFs $A_2BM_3F_{12}$ ($M^{3+} = Ti^{3+}, V^{3+}$) provide a good stage to systematically study the effect of combination of spin frustration and quantum fluctuation in the case of $S = 1/2$ and $S = 1$, which is very rare in the real kagome system.

In this paper, we report crystal structure and magnetic properties of $S = 1$ KLAFs $A_2BV_3F_{12}$ with Ising-like anisotropy. KLAFs $A_2BV_3F_{12}$ have slightly distorted kagome lattices. The magnetization and magnetic susceptibility are highly anisotropic. KLAFs $A_2BV_3F_{12}$ form antiferromagnetic ordering with distorted 120° structure or other nearly coplanar magnetic structure at low temperatures whose basal spin plane is perpendicular to the kagome plane. The high field magnetization curves show distinct 1/3 and 2/3 magnetization plateaus when magnetic fields are applied perpendicular to the kagome plane. Moreover, jumps of the magnetization with hysteresis are observed for $Rb_2NaV_3F_{12}$ under in-plane magnetic fields. We discuss the magnetic properties of $A_2BV_3F_{12}$ and the origins of the magnetic field induced phase transitions.

II. EXPERIMENT

Single crystals of $A_2BV_3F_{12}$ were grown using flux methods in Ni crucibles under Ar atmosphere. Dried alkali metal fluorides AF and BF and purified VF_3 were used as the starting materials. Mixtures of alkali metal chlorides were used as fluxes.

X-ray diffraction data of obtained crystals were collected at 120 K using BL8A beamline with a wavelength of 0.68901 Å ($Cs_2KV_3F_{12}$) or 0.68938 Å ($Cs_2NaV_3F_{12}$ and $Rb_2NaV_3F_{12}$) at the Photon Factory, KEK (Japan). In the measurements, we used crystals with a typical size of $80 \times 40 \times 20$ μm^3. For $Cs_2KV_3F_{12}$ and $Cs_2NaV_3F_{12}$, preformed domains exist, and thus we analyzed the data by considering the contributions of consisting domains. The structural parameters were refined using a full-matrix least-squares method with the SHELXL-97 software [31].

All the physical properties of $A_2BV_3F_{12}$ reported in this paper were measured using crystals. dc magnetization measurements were performed in a temperature range of 2–350 K using a superconducting quantum interference device magnetometer (Quantum Design MPMS-XL system) in the Research Center for Low Temperature and Materials Sciences, Kyoto University. Magnetization curves up to approximately 60 T were measured using an induction method with a multilayer pulsed magnet at the International MegaGauss Science Laboratory of the Institute for Solid State Physics at the University of Tokyo. In these magnetization measurements, magnetic field H was applied along several directions. For $Rb_2NaV_3F_{12}$, domain-free single crystals are obtained, and thus we performed the measurements for $H \perp ab$, $H \parallel a$, and $H \parallel b$. For $Cs_2KV_3F_{12}$ and $Cs_2NaV_3F_{12}$, crystals consist of domains by sharing the ab plane, and thus we performed the measurements for $H \perp ab$ and $H \parallel ab$. Heat capacity measurements were performed with a relaxation method using a Quantum Design PPMS-14LHS.

TABLE I. Structural parameters of $A_2BV_3F_{12}$ at 120 K, along with the respective space groups, lattice parameters a, b, c, and β, number of the formula unit in the unit cell Z, range for data integration θ, the number of the reflection which satisfies the condition "$F_0 > 4\sigma(F_0)$" N, and the residual indices R, ωR. For $Cs_2NaV_3F_{12}$ and $Rb_2NaV_3F_{12}$, the structural parameters were refined including anisotropic displacement parameters. The numbers in parentheses are standard deviations in the last significant figures.

	$Cs_2KV_3F_{12}$	$Cs_2NaV_3F_{12}$	$Rb_2NaV_3F_{12}$
Space group	$P2_1/c$	$P2_1/m$	$P2_1/m$
a (Å)	12.925(2)	12.789(3)	12.578(6)
b (Å)	7.467(4)	7.433(3)	7.414(3)
c (Å)	15.028(9)	7.385(3)	7.1922(12)
β (deg)	124.83(3)	125.67(2)	126.256(12)
Z	4	2	2
θ	3.09–59.44	3.27–59.50	2.75–59.47
N	8757	6612	3352
R	0.0464	0.0221	0.0150
ωR	0.1290	0.0591	0.0382

III. RESULTS

A. Crystal structures

In our systematic studies of fluorides, we discovered three $S = 1$ kagome fluorides $A_2BV_3F_{12}$ ($Rb_2NaV_3F_{12}$, $Cs_2NaV_3F_{12}$, and $Cs_2KV_3F_{12}$) in addition to previously reported $S = 1/2$ three Ti^{3+} fluorides $A_2BTi_3F_{12}$ [23]. We succeeded in growing their hexagonal-shaped single crystals with a typical size of $2.0 \times 2.0 \times 0.8$ mm^3. For $Cs_2NaV_3F_{12}$ and $Cs_2KV_3F_{12}$, the crystals consist of some domains by sharing the kagome planes, as revealed by x-ray diffraction and polarizing microscope measurements. The crystals are purple ($Cs_2KV_3F_{12}$) or brown ($Cs_2NaV_3F_{12}$ and $Rb_2NaV_3F_{12}$), indicating that they are insulators. The structural parameters are listed in Table I. The atomic coordinates and the isotropic displacements of $Cs_2KV_3F_{12}$, $Cs_2NaV_3F_{12}$, and $Rb_2NaV_3F_{12}$ are collected in Tables II, III, and IV, respectively. While $Cs_2NaV_3F_{12}$ and $Rb_2NaV_3F_{12}$ crystallize in a monoclinic system of $P2_1/m$ as well as $A_2BTi_3F_{12}$ [23], $Cs_2KV_3F_{12}$ possesses lower symmetry of $P2_1/c$ with doubling of the unit cell along the c axis, as shown in Figs. 1(a) and 1(d). Note that $P2_1/c$ can be clearly distinguished from $P2_1/m$ by the extinction rule of $l \neq 2n + 1$ for $h0l$. The atomic arrangement of $Cs_2NaV_3F_{12}$ and $Rb_2NaV_3F_{12}$ is qualitatively the same as that of $Cs_2KV_3F_{12}$, resulting in the quite similar overall appearances among three compounds of $A_2BV_3F_{12}$. The crystal structure of $A_2BV_3F_{12}$ can be understood

TABLE II. Atomic coordinates and isotropic displacement parameters in $Cs_2KV_3F_{12}$. The numbers in parentheses are standard deviations in the last significant figures.

Atom	x	y	z	U (Å^2)
Cs1	0.623623(11)	0.767937(15)	0.317388(9)	0.01195(3)
Cs2	0.137339(9)	0.219657(12)	0.821945(8)	0.01046(3)
K1	0.75149(2)	0.23146(2)	0.76072(2)	0.00689(4)
V1	0	0	0	0.00345(5)
V2	0.5	0	0	0.00333(5)
V3	0.763708(12)	0.25016(3)	0.020860(10)	0.00450(3)
V4	0	0.5	0	0.00348(5)
V5	0.5	0.5	0	0.00368(5)
F1	0.00688(5)	0.25120(13)	0.95916(5)	0.00670(7)
F2	0.55188(6)	0.47691(13)	0.14422(5)	0.01062(8)
F3	0.15297(5)	0.94132(12)	0.00969(5)	0.00772(7)
F4	0.10412(6)	0.05292(10)	0.14942(6)	0.01014(8)
F5	0.55773(5)	0.74764(14)	0.02603(5)	0.00810(8)
F6	0.32490(5)	0.56958(10)	0.95079(5)	0.00754(7)
F7	0.12958(7)	0.70132(14)	0.33040(7)	0.01040(10)
F8	0.34379(8)	0.70950(12)	0.12830(8)	0.01161(11)
F9	0.57854(7)	0.46829(14)	0.64791(6)	0.01263(9)
F10	0.11860(5)	0.93616(10)	0.46126(6)	0.00882(7)
F11	0.13852(5)	0.46081(10)	0.14466(5)	0.00950(8)
F12	0.34564(6)	0.93938(12)	0.98800(5)	0.00841(7)

as ordered structure of the cubic modified pyrochlore $RbNiCrF_6$-type structure [32]. Magnetic V^{3+} ions with t_{2g}^2 electron configuration are octahedrally coordinated by F atoms and form slightly distorted kagome lattices in the ab plane [see Figs. 1(b) and 1(e)]. As shown in Figs. 1(a) and 1(d), the V^{3+} kagome layers are slightly undulated perpendicular to the ab plane, and the amount of undulation is evaluated by the value $cz \sin\beta$ of V3 (0.25–0.57 Å). Although slight undulation is present, the kagome layers are well separated by the layers of the nonmagnetic large alkali metal ions of A^+ and B^+. Then, the superexchange paths between the kagome

TABLE III. Atomic coordinates and equivalent isotropic displacement parameters in $Cs_2NaV_3F_{12}$. The numbers in parentheses are standard deviations in the last significant figures.

Atom	x	y	z	U_{eq} (Å^2)
Cs1	0.61684(6)	0.75	0.622868(10)	0.01125(1)
Cs2	0.136454(6)	0.25	0.619063(8)	0.01008(1)
Na1	0.74383(3)	0.25	0.52852(6)	0.00623(4)
V1	0	0	0	0.00432(2)
V2	0.5	0	0	0.00409(2)
V3	0.773577(10)	0.25	0.066635(16)	0.00422(2)
F1	0.01072(6)	0.25	0.93003(9)	0.01056(8)
F2	0.57587(4)	0.44888(5)	0.30202(5)	0.00978(5)
F3	0.10416(4)	0.93481(4)	0.89085(6)	0.00865(4)
F4	0.15077(3)	0.02636(6)	0.28987(5)	0.01037(5)
F5	0.55957(5)	0.75	0.08458(9)	0.00815(6)
F6	0.33725(4)	0.55377(5)	0.95803(7)	0.01024(5)
F7	0.14540(6)	0.75	0.62296(8)	0.01239(9)
F8	0.31698(6)	0.75	0.24263(9)	0.01160(8)

TABLE IV. Atomic coordinates and equivalent isotropic displacement parameters in $Rb_2NaV_3F_{12}$. The numbers in parentheses are standard deviations in the last significant figures.

Atom	x	y	z	U_{eq} (Å^2)
Rb1	0.605635(10)	0.75	0.59046(2)	0.00963(3)
Rb2	0.140822(11)	0.25	0.60978(3)	0.01135(4)
Na1	0.74051(5)	0.25	0.53689(11)	0.00767(11)
V1	0	0	0	0.00424(5)
V2	0.5	0	0	0.00384(4)
V3	0.784781(16)	0.25	0.09882(4)	0.00422(5)
F1	0.99403(8)	0.25	0.91088(16)	0.00896(16)
F2	0.55549(5)	0.44362(6)	0.29924(12)	0.00940(12)
F3	0.09471(5)	0.93824(5)	0.86650(11)	0.00846(12)
F4	0.16141(5)	0.03875(6)	0.29051(11)	0.00928(12)
F5	0.56064(7)	0.75	0.10585(15)	0.00749(16)
F6	0.32385(5)	0.55385(6)	0.91007(12)	0.01025(12)
F7	0.12436(8)	0.75	0.58060(18)	0.01267(18)
F8	0.31655(7)	0.75	0.22132(17)	0.01035(17)

planes V-F-A(B)-F-V are very difficult to connect, which produces a quasi-2D kagome lattice.

Owing to the small distortion of kagome lattices originating from the monoclinic structure, KLAFs $A_2BV_3F_{12}$ have several crystallographically different V^{3+} sites, which depend on the space group. As shown in Figs. 1(a) and 1(b), $Cs_2NaV_3F_{12}$ and $Rb_2NaV_3F_{12}$ have three V^{3+} sites. Both V1 and V2 form

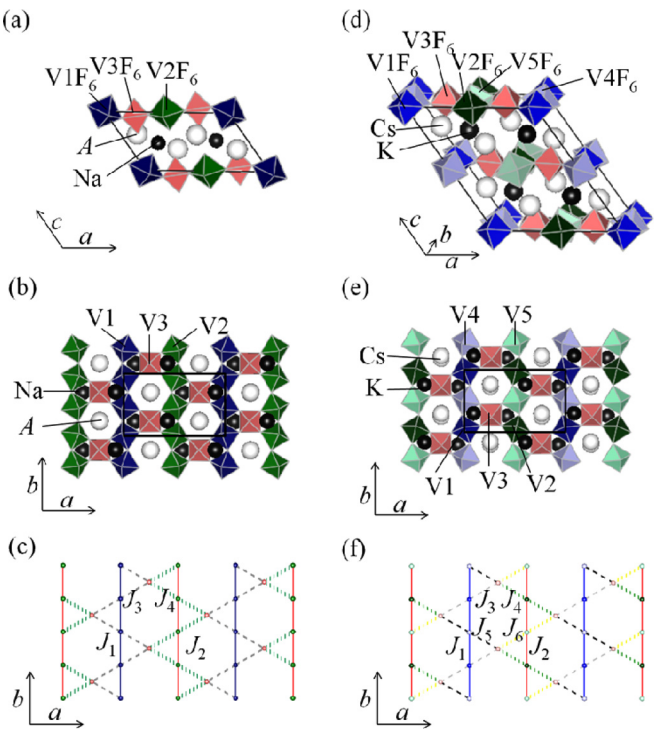

FIG. 1. Crystal structure of $Cs_2NaV_3F_{12}$ and $Rb_2NaV_3F_{12}$ viewed (a) along the b axis, and (b) perpendicular to the ab plane. The crystal structure of $Cs_2KV_3F_{12}$ viewed (d) approximately along the b axis and (e) perpendicular to the ab plane. Black lines show the unit cell. Exchange network in the kagome layer (c) for $A_2BTi_3F_{12}$, $Cs_2NaV_3F_{12}$, and $Rb_2NaV_3F_{12}$ and (f) for $Cs_2KV_3F_{12}$.

one-dimensional chains along the b axis and the chains of V1 and V2 are bridged by V3. Consequently, as shown in Fig. 1(c), $Cs_2NaV_3F_{12}$ and $Rb_2NaV_3F_{12}$ have four types of the exchange interactions between nearest neighbor V atoms: V1-V1, V2-V2, V1-V3, and V2-V3, which are denoted as J_1, J_2, J_3, and J_4, respectively. For $Cs_2KV_3F_{12}$, accompanied with doubling of the unit cell along the c axis, two V^{3+} sites are present in each V chain along the b axis, which is shown in Figs. 1(d) and 1(e). Hence $Cs_2KV_3F_{12}$ has five V^{3+} sites in each kagome plane and has six types of exchange interactions J_1, J_2, J_3, J_4, J_5, and J_6, as shown in Fig. 1(f). Here, each VF_6 octahedron is flattened along one F-V-F direction that is roughly perpendicular to the ab plane in $A_2BV_3F_{12}$. Thus the superexchange interaction paths through F atoms are considered to be nearly equivalent in the in-plane exchange interactions J_i ($i = 1,2,\ldots$). This fact suggests that the superexchange interactions mainly depend on ∠V-F-V, V-V distance, and so on. The average bond angles of the superexchange interactions ∠V-F-V are 143.0° for $Cs_2KV_3F_{12}$, 142.4° for $Cs_2NaV_3F_{12}$, and 141.0° for $Rb_2NaV_3F_{12}$. In each compound, the difference between the largest and the smallest bond angle ∠V-F-V is less than 6°. The difference between the largest and the smallest bond length among nearest neighbor V atoms is 0.2% for $Cs_2KV_3F_{12}$, 0.6% for $Cs_2NaV_3F_{12}$, and 0.7% for $Rb_2NaV_3F_{12}$. Please note that the distortion of framework of kagome lattices in $A_2BV_3F_{12}$ is relatively small compared with other distorted kagome compounds from the crystal structural parameters. For example, the distortion in $A_2BV_3F_{12}$ is much smaller than that in volborthite [33]. The difference of bond length V-V in $Cs_2KV_3F_{12}$ is as small as that in $BaCu_3V_2O_8(OH)_2$ (Cu-Cu: 0.07%–0.2%) [34]. Small differences of ∠V-F-V and the bond length V-V suggest that all exchange interactions between nearest neighbor V ions have the same sign in $A_2BV_3F_{12}$. The values $cz\sin\beta$ of V3 and the difference of bond length V-V indicate that the distortion of kagome lattice becomes small as the ionic radii of A and B increase, which is the same as $A_2BTi_3F_{12}$ [23]. Small distortion can affect the exchange interactions J_i and the magnitude of single ion-magnetic anisotropy.

B. Magnetic properties at low magnetic fields

Figure 2 shows temperature T dependence of magnetic susceptibility $\chi = M/H$ and its inverse χ^{-1} under $\mu_0 H = 1$ T for $H \perp ab$ and $H \parallel ab$, where M is the magnetization, H is a magnetic field, μ_0 is the vacuum magnetic permeability, and ab corresponds to the kagome plane. At high temperatures, the χ-T curves of three compounds are similar and show Curie-Weiss like behaviors. Large magnetic anisotropy of χ is observed in all temperature regions. The $\chi^{\perp ab}$ values are larger than the $\chi^{\parallel ab}$ values in $T \gtrsim 300$ K and $T \lesssim 15$ K, and vice versa. The large magnetic anisotropy is mainly due to distortion of VF_6 octahedra and large spin-orbit interaction originating from partially unquenched orbital magnetic moments of V^{3+}. The effect of magnetic anisotropy can be mainly divided into three factors: anisotropic g factors, large anisotropic van Vleck paramagnetic susceptibility, and single ion-magnetic anisotropy. The van Vleck paramagnetic susceptibility χ_v^i ($i = \perp ab, a, b$) is approximately proportional to $2 - g^i$. Axial single ion-magnetic anisotropy energy is expressed as $DS^2_{\perp ab}$, and the coefficient D is roughly proportional to $\{g^{\perp ab} - (g^a + g^b)/2\}$. Please note that χ_v, g, and D show small T dependence when T is as large as the coefficient of spin-orbit interaction $\lambda = 105$ cm^{-1} [35] for V^{3+}. Thus g, Weiss temperature θ_{CW}, and χ_v obtained from the Curie-Weiss fitting are only advisory. However, the obtained parameters give qualitatively important results in $A_2BV_3F_{12}$ including Ising-like single ion-magnetic anisotropy, which are shown in the next paragraph.

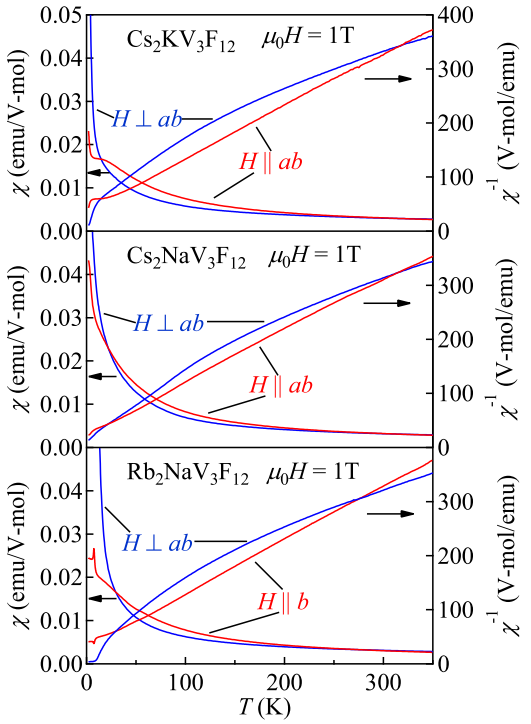

FIG. 2. Temperature dependence of the magnetic susceptibility $\chi = M/H$ and their inverses χ^{-1} of $A_2BV_3F_{12}$ under $\mu_0 H = 1$ T for $H \perp ab$ and $H \parallel ab$ ($H \parallel b$ for $Rb_2NaV_3F_{12}$). All the measurements were performed under field cooling conditions.

At high temperatures, the χ^{-1}-T curves for $H \parallel ab$ are almost linear, while χ^{-1}-T curves for $H \perp ab$ are clearly upwardly convex. The modified Curie-Weiss fittings $\chi = C/(T - \theta_{CW}) + \chi_0$ between 150 and 350 K give values of g, θ_{CW}, and χ_v. The results of the fittings are shown in Table V. As mentioned above, these estimated parameters are only advisory. Indeed, these parameters strongly depend on the fitting range. However, these parameters always satisfy the relations $\theta_{CW} < 0$, $g^{\perp ab} < g^{a,b} \sim 2$, and $\chi_0^{a,b} \ll \chi_0^{\perp ab}$ irrespective of the fitting range. Negative θ_{CW} values indicate dominant antiferromagnetic interactions in $A_2BV_3F_{12}$. The relations $g^{\perp ab} < g^{a,b} \sim 2$ and $\chi_0^{a,b} \ll \chi_0^{\perp ab}$, which correspond to $\chi_v^{a,b} \ll \chi_v^{\perp ab}$, are consistent with roughly linear χ^{-1}-T curves for $H \parallel ab$ and upwardly convex ones for $H \perp ab$. In addition, $D < 0$ is expected from the relation $g^{\perp ab} < g^{a,b}$, which means the presence of Ising-like single ion-magnetic anisotropy along the $\perp ab$ direction in $A_2BV_3F_{12}$. In $T \lesssim 15$ K, the effect of Ising-like anisotropy becomes larger, and hence spin moments tend to point parallel to the $\perp ab$ direction, which causes enhancement of $\chi^{\perp ab}$ and suppression of $\chi^{\parallel ab}$ in $A_2BV_3F_{12}$. Thus the $\chi^{\perp ab}$ value is larger than the $\chi^{\parallel ab}$ value

TABLE V. Characteristic parameters $p_{\rm eff}$, g factors for $S = 1$, $\theta_{\rm CW}$, and χ_0 obtained from the modified Curie-Weiss fitting $\chi = C/(T - \theta_{\rm CW}) + \chi_0$ between 150 and 350 K are listed, where $p_{\rm eff} = \sqrt{8C} = \sqrt{2}g$. Although these parameters are only advisory, the relations $\theta_{\rm CW} < 0$, $g^{\perp ab} < g^{a,b}$, and $\chi_0^{a,b} \ll \chi_0^{\perp \rm ab}$ are always satisfied irrespective of the fitting range.

	$H \parallel ab$				$H \perp ab$			
	$p_{\rm eff}$	g	$\theta_{\rm CW}$ (K)	χ_0 (emu/mol)	$p_{\rm eff}$	g	$\theta_{\rm CW}$ (K)	χ_0 (emu/mol)
$Cs_2KV_3F_{12}$	2.59	1.83	−16	4.0×10^{-4}	2.34	1.66	−50	1.1×10^{-3}
$Cs_2NaV_3F_{12}$	2.59	1.83	−7	4.8×10^{-4}	2.33	1.65	−21	1.1×10^{-3}
$Rb_2NaV_3F_{12}$	2.70	1.90	−19	1.8×10^{-4}	2.26	1.59	−29	1.2×10^{-3}

in $T \lesssim 15$ K. The Ising-like anisotropy plays a very important role in the magnetic properties of $A_2BV_3F_{12}$.

As shown in Fig. 2, each χ value for $H \parallel ab$ tends to approach a constant value with decreasing T below 15 K owing to Ising-like anisotropy along the $\perp ab$ direction and then starts to increase rapidly at a certain temperature. The rapid increases of χ suggest the presence of magnetic phase transitions. Thus we measured T dependence of heat capacity C of $A_2BV_3F_{12}$, the results of which are shown in Fig. 3. The C/T-T curves of $Cs_2KV_3F_{12}$ and $Rb_2NaV_3F_{12}$ show sharp λ-typed peaks and that of $Cs_2NaV_3F_{12}$ shows a somewhat broad peak at low temperatures. Peaks of C/T-T indicate magnetic phase transitions. We define the transition temperature $T_{\rm N}$ as the minimum point of $\frac{d(C/T)}{dT}$-T, and we get $T_{\rm N}$ of 2.5, 4.9, and 8.0 K for $Cs_2KV_3F_{12}$, $Cs_2NaV_3F_{12}$, and $Rb_2NaV_3F_{12}$, respectively. In addition, as shown in Fig. 4, C/T-T for $Cs_2NaV_3F_{12}$ shows a cusp at approximately 80 K, and C/T decreases linearly between 40 and 80 K, which suggests a change of the electric state in the T range. The strange behavior is possibly related to the broad peak of C/T-T for $Cs_2NaV_3F_{12}$ around $T_{\rm N}$.

In order to examine the magnetic states below $T_{\rm N}$ in detail, we measured M/H-T curves under several H for $H \perp ab$ and $H \parallel ab$ as shown in Fig. 5, which also indicates the presence of magnetic ordering. In the three compounds, M/H-T depends on H at low temperatures for both $H \perp ab$ and $H \parallel ab$. Under 5 T, each M/H increases monotonically with decreasing T. With decreasing H, each M/H increases at the same T. In addition, under 0.1 T, each M/H under the zero field cooling condition deviates from that under the field cooling condition at low temperatures as shown in the insets of Fig. 5, which is often observed in magnetically ordered systems. Each deviation temperature is lower than $T_{\rm N}$. Although no deviation is observed in $Cs_2KV_3F_{12}$ ($T_{\rm N} = 2.5$ K) for $H \perp ab$, we think that the deviation would be observed below 2 K. Accompanied with magnetic ordering, larger anisotropy of M/H appears in the three compounds. Below $T_{\rm N}$, each M/H value for $H \perp ab$ is obviously larger than that for $H \parallel ab$ under the same H. Anisotropy of M/H becomes larger in the order of $Cs_2NaV_3F_{12}$, $Cs_2KV_3F_{12}$, and $Rb_2NaV_3F_{12}$, which does not correspond to the order of distortion of the framework of kagome lattice. The origin of the difference is discussed in the next section. In particular, for $Rb_2NaV_3F_{12}$ with the largest anisotropy of M/H, magnetic anisotropy in the ab plane is also observed. For $H \parallel a$, M/H increases monotonically with decreasing T. For $H \parallel b$, M/H-T shows a sharp peak at 7.5 K ($\sim T_{\rm N}$) under 0.1 and 1 T.

In addition to the M/H-T data, the M-H curves help us to clarify the magnetic states below $T_{\rm N}$. As shown in Fig. 6, in the three compounds, each M value for $H \perp ab$ is clearly larger than that for $H \parallel ab$ up to 4 T below $T_{\rm N}$, which is consistent with the M/H-T data. Moreover, magnetic anisotropy of M becomes larger in the order of $Cs_2NaV_3F_{12}$, $Cs_2KV_3F_{12}$, and $Rb_2NaV_3F_{12}$. In particular, the M-H curves of $Cs_2KV_3F_{12}$ and $Rb_2NaV_3F_{12}$ for $H \perp ab$ show spontaneous magnetization $M_{\rm sp} \sim 0.1\mu_{\rm B}$ and $M_{\rm sp} \sim 0.4\mu_{\rm B}$, respectively.

The M/H-T and M-H data can be compared with theoretical studies of KLAFs with Ising anisotropy. Contrary to the ideal Heisenberg KLAFs and Ising KLAFs, Heisenberg-like KLAFs with Ising anisotropy were predicted to show a magnetic phase transition with $M_{\rm sp}$ along the easy axis at finite temperature owing to the breaking of twofold symmetry [16]. Below the critical temperature, although long range ordering of the sublattice was predicted to be absent, three spins on each triangle were considered to form a distorted 120° structure whose spin plane included the easy axis [16]. Thus, below

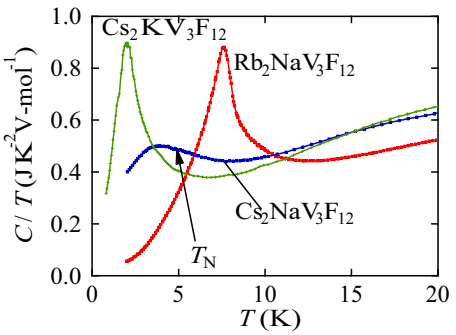

FIG. 3. Temperature dependence of the heat capacity divided by temperature C/T of $A_2BV_3F_{12}$ below 20 K.

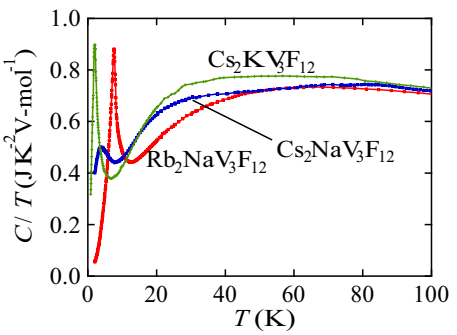

FIG. 4. Temperature dependence of the heat capacity divided by temperature C/T of $A_2BV_3F_{12}$ below 100 K.

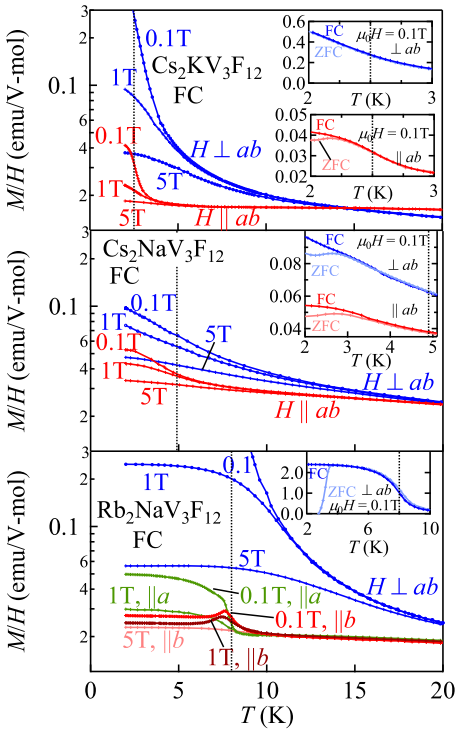

FIG. 5. Main panels: temperature dependence of M/H under 0.1, 1, and 5 T for $H \perp ab$, $H \parallel a$, and $H \parallel b$. Dashed lines indicate the magnetic phase transition temperatures T_N determined by the heat capacity measurement. All the measurements were performed under field cooling conditions. The insets: M/H-T curves at 0.1 T under both field and zero field cooling conditions are plotted.

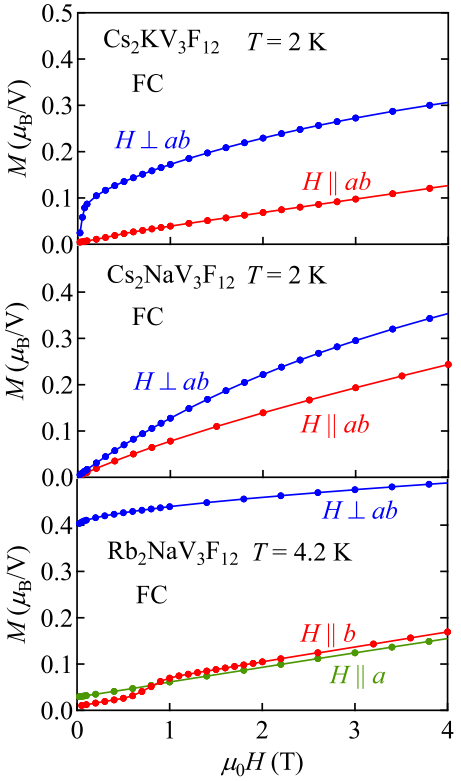

FIG. 6. Magnetization curves up to 4 T for $H \perp ab$, $H \parallel a$, and $H \parallel b$ at 2 or 4.2 K. All the measurements were performed under field cooling conditions. M-H curves at 4.2 K are plotted for $Rb_2NaV_3F_{12}$, while those at 2 K are plotted for $Cs_2NaV_3F_{12}$ and $Cs_2KV_3F_{12}$.

the critical temperature at low magnetic fields, the M value under easy axis fields is considered to be larger than that under in-plane fields.

Although KLAFs $A_2BV_3F_{12}$ with Ising-like anisotropy show long-range magnetic ordering, the M-H data are very similar to the above situation. Thus it is likely that the ground states of $A_2BV_3F_{12}$ are a distorted 120° structure whose basal spin plane is perpendicular to the kagome plane, since the easy axis is perpendicular to the kagome plane. Otherwise, in quasi-two-dimensional antiferromagnets $A_2BV_3F_{12}$, the ground states are considered to be nearly coplanar magnetic structures whose basal spin plane is perpendicular to the kagome plane. In particular, M_{sp} for $Cs_2KV_3F_{12}$ and $Rb_2NaV_3F_{12}$ suggests that spin canting along the easy axis occurs in the basal spin plane, reflecting larger anisotropy of M. Moreover, different values of J help long-range magnetic ordering in $A_2BV_3F_{12}$. In KLAFs with two exchange interactions J and J', a ferrimagnetic state or a large manifold of canted spin states can arise in a certain range of J/J', which depends on the quantum spin number S [36,37]. Thus magnetic ordering with canted spin states in $A_2BV_3F_{12}$ is stabilized by the combination of Ising-like anisotropy and different values of J.

As mentioned before, $Rb_2NaV_3F_{12}$ with the largest anisotropy of M among $A_2BV_3F_{12}$ shows ab-plane magnetic anisotropy, which suggests the presence of in-plane single ion-magnetic anisotropy $E(S^2_{\parallel a} - S^2_{\parallel b})$ and supports a nearly coplanar magnetic structure. As shown in Fig. 6, M for $H \parallel b$ jumps at approximately 0.8 T, while M-H for $H \parallel a$ shows $M_{sp} \sim 0.03\mu_B$. Moreover, Fig. 7 shows the M-H curves of $Rb_2NaV_3F_{12}$ at 4.2 K including both H increasing and decreasing processes. For $H \parallel a$, a hysteresis loop with $M_{sp} \sim 0.03\mu_B$ is observed between -0.8 and 0.8 T, and M-H is linear above 0.8 T. For $H \parallel b$, M jumps at approximately 1.1 T in the H-increasing process, whereas M jumps at 0.8 T in the H-decreasing process. Above 2 T, M-H for $H \parallel b$ roughly coincides with that for $H \parallel a$. The M-H curves for $H \parallel a$ and $H \parallel b$ suggest that all V^{3+} spins in the ground state are basically arranged perpendicular to the a axis, which is consistent with the picture of nearly coplanar

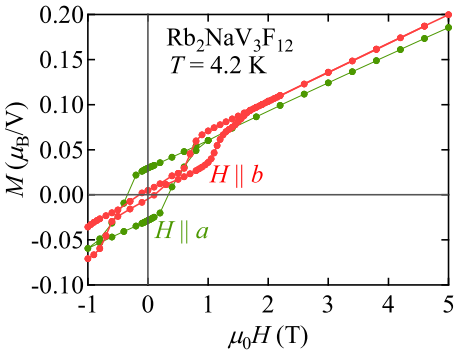

FIG. 7. Magnetization curves of $Rb_2NaV_3F_{12}$ between -1 and 5 T at 4.2 K for $H \parallel a$ and $H \parallel b$. The measurement for $H \parallel a$ ($H \parallel b$) was performed from 5 T to -1 T (5 T to -5 T) and from -1 T to 5 T (-5 T to 5 T).

magnetic structure. From $M_{sp} \sim 0.03\mu_B$ for $H \parallel a$, all spins are considered to slightly cant to the a axis in the ground state. The direction of the basal spin plane suggests $E > 0$ in $E(S^2_{\parallel a} - S^2_{\parallel b})$. Slight spin canting along the a axis is possibly due to the DM interaction and/or magnetocrystalline anisotropy. In addition, the jump of M for $H \parallel b$ around 1 T is considered to correspond to a sort of spin flop ($E \sim 1\mu_B$T). Thus, above 2 T for $H \parallel b$, the basal spin plane includes the a axis and all V^{3+} spins slightly cant to the b axis. The above picture is consistent with the M/H-T data.

C. High field magnetization

From the χ-T, C/T-T, and M-H data, it is confirmed that each compound of $A_2BV_3F_{12}$ shows an antiferromagnetic transition at low temperatures. The magnetic structure below T_N is suggested to be distorted 120° structure or other nearly coplanar magnetic structure whose basal spin plane is perpendicular to the kagome plane. In KLAFs $A_2BV_3F_{12}$ with Ising-like anisotropy, exotic magnetic phenomena such as a 1/3 magnetization plateau are expected under high magnetic fields. Figure 8 shows M-H curves of $A_2BV_3F_{12}$ up to approximately 60 T at 1.3 and 4.2 K. The M-H curves are highly anisotropic in three compounds even under high magnetic fields. As shown in Figs. 8(b), 8(d), and 8(f), the M-H curves for $H \perp ab$ show 1/3 and 2/3 magnetization plateaus. In contrast for $H \parallel ab$, as shown in Figs. 8(a), 8(c), 8(e), and 8(g), no distinct plateau is observed in three compounds, and instead jumps of M with hysteresis are observed for $Rb_2NaV_3F_{12}$.

As mentioned above, for $H \perp ab$, the M-H curves of $A_2BV_3F_{12}$ show 1/3 and 2/3 magnetization plateaus. The M-H curves of the three compounds are similar. The magnetization M in the three compounds saturates at about 50 T, and the saturation magnetization M_{sat} is estimated to be $1.47\mu_B$ for $Cs_2KV_3F_{12}$, $1.65\mu_B$ for $Cs_2NaV_3F_{12}$, and $1.62\mu_B$ for $Rb_2NaV_3F_{12}$. The M_{sat} values are much smaller than $2\mu_B$ for $S = 1$ and $g = 2$, which is consistent with the χ-T data. As shown in Fig. 8(b), M for $Cs_2KV_3F_{12}$ at 1.3 K increases upwardly convexly with increasing $\mu_0 H$ from 0 T, and becomes almost constant between 9 and 16 T, which corresponds to a 1/3 magnetization plateau. The arrangements of V^{3+} spins with increasing $\mu_0 H$ are expected as follows. In the ground state of $Cs_2KV_3F_{12}$, spin canting along the $\perp ab$ direction occurs in the basal spin plane. With increasing $\mu_0 H$ for $H \perp ab$, the magnitude of spin canting becomes large. In the 1/3 magnetization-plateau state, up up down spin structure is considered to be realized in each V^{3+} triangle, as is observed in $S = 7/2$ TLAFs $GdPd_2Al_3$ [28]. With further increasing $\mu_0 H$ from 16 T, M starts to increase gradually and increases rapidly at 23 T, and then the slope of dM/dH becomes small and almost constant between 30 and 35 T, which corresponds to a 2/3 magnetization plateau. In the 2/3 magnetization-plateau state, one-half of down spins in the 1/3 magnetization-plateau state are considered to change to up spins, although the detailed arrangement of V^{3+} spins is unclear. These two magnetization plateaus are also confirmed by two broad minima of dM/dH-H, which approximately correspond to $M/M_{sat} = 1/3$ and 2/3 as indicated by gray lines in Fig. 8(b). After the 2/3 magnetization plateau, M increases rapidly at

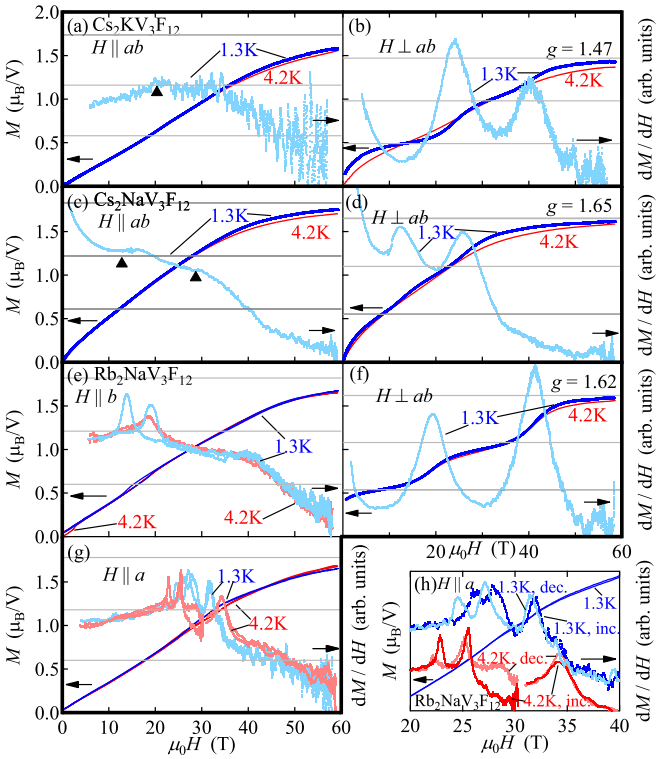

FIG. 8. Magnetization curves M-H and the differential magnetization curves dM/dH-H up to approximately 60 T in $A_2BV_3F_{12}$ at 1.3 and 4.2 K for $H \perp ab$, $H \parallel a$, and $H \parallel b$ are displayed. The horizontal gray lines indicate $M = 1/3M_{sat}$, $M = 2/3M_{sat}$, and $M = M_{sat}$, where $M_{sat} = g\mu_B$ is the saturation magnetization. Since M for $H \parallel ab$ seems not to saturate even at 60 T and errors of the estimated g factors are large, g factors for $H \perp ab$ are only displayed. Triangular markers indicate anomalies of the dM/dH-H curves in $Cs_2KV_3F_{12}$ and $Cs_2NaV_3F_{12}$. Figure (h) shows enlarged M-H and dM/dH-H curves around the anomalies for $H \parallel a$ in $Rb_2NaV_3F_{12}$. The terms "inc." and "dec." indicate the data with increasing H and decreasing H, respectively.

40 T and then saturates to $M_{sat} \sim 1.47\mu_B$ at 50 T. Similarly, as shown in Figs. 8(d) and 8(f), the dM/dH-H curves for $Cs_2NaV_3F_{12}$ and $Rb_2NaV_3F_{12}$ show two broad minima at $M/M_{sat} = 1/3$ and 2/3, which confirm the presence of 1/3 and 2/3 magnetization plateaus. The 1/3 and 2/3 magnetization plateaus become more distinct in the order of $Cs_2NaV_3F_{12}$, $Cs_2KV_3F_{12}$, and $Rb_2NaV_3F_{12}$, which corresponds to the order of the smallest anisotropy of M. These magnetization plateaus are the most impressive observations in $A_2BV_3F_{12}$. Even at 4.2 K, 1/3 and 2/3 magnetization plateaus are observed in the three compounds. For $Rb_2NaV_3F_{12}$, the M-H curve at 4.2 K is almost the same as that at 1.3 K, reflecting large $T_N = 8.0$ K. In contrast for $Cs_2KV_3F_{12}$ and $Cs_2NaV_3F_{12}$, the two magnetization plateaus are less distinct at 4.2 K. Moreover, the plateaus for $Cs_2KV_3F_{12}$ are observed even above $T_N = 2.5$ K.

Unlike the M-H curves for $H \perp ab$, the M-H curves for $H \parallel ab$ show no distinct plateau. As shown in Fig. 8, each estimated g factor for $H \parallel ab$ is obviously larger than that for $H \perp ab$, which is consistent with $D < 0$ (Ising-like single ion anisotropy) based on the χ-T data. The M-H curves for $H \parallel ab$ are qualitatively different in the three compounds. The

details are described in the order of the smallest anisotropy. As shown in Fig. 8(c), dM/dH for $Cs_2NaV_3F_{12}$ at 1.3 K decreases monotonically with increasing $\mu_0 H$ from 0 to 60 T. However, two dM/dH-constant regions are observed around 12 and 29 T, which roughly correspond to $M/M_{sat} = 1/3$ and 2/3, respectively. These regions might be signs of 1/3 and 2/3 magnetization plateaus. In contrast for $Cs_2KV_3F_{12}$, dM/dH at 1.3 K slightly increases with increasing $\mu_0 H$ and then becomes almost constant at $M/M_{sat} = 1/3$ (20 T). With further increasing $\mu_0 H$, dM/dH starts to decrease at 35 T, and M gradually approaches saturation.

In particular, for $Rb_2NaV_3F_{12}$, the M-H curves for $H \parallel a$ and $H \parallel b$ show unique behaviors. As shown in Fig. 8(e), for $H \parallel b$, M at 1.3 K increases roughly linearly from 0 T and then jumps at 20 T in the increasing process and at 14 T in the decreasing process, while M at 4.2 K jumps at 20 T without hysteresis. The positions of these jumps roughly correspond to $M/M_{sat} = 1/3$, which suggests destabilization of the 1/3 magnetization-plateau state. As shown in Fig. 8(g), while the M-H curves for $H \parallel a$ at 1.3 and 4.2 K show no anomaly at $M/M_{sat} = 1/3$, three anomalies with hysteresis are observed near $M/M_{sat} = 2/3$, which are enlarged in Fig. 8(h). The dM/dH-H curve at 1.3 K shows three peaks at 26, 28, and 32 T in the increasing process. At 4.2 K, the peak position of dM/dH-H at the highest H shifts to higher H side, while those of the other two peaks shift to lower H side. The jumps of M seem to destabilize the 2/3 magnetization-plateau state. For $Rb_2NaV_3F_{12}$, as shown in Fig. 7, the M-H curves for $H \parallel a$ and $H \parallel b$ are almost the same above 2 T. Nevertheless, surprisingly, in-plane magnetic anisotropy is again observed under high magnetic fields, which suggests emergence of high field phases for $H \parallel a$ and $H \parallel b$ independently. Thus KLAFs $A_2BV_3F_{12}$ show various behaviors in the M-H curves for $H \parallel ab$ owing to the difference of anisotropy. In addition, these M-H curves for $H \parallel ab$ suggest that Ising-like single ion anisotropy is one of the most important factors to stabilize the magnetization-plateaus state in $A_2BV_3F_{12}$.

IV. DISCUSSION

As mentioned before, we discovered three kagome fluorides $S = 1$ V^{3+} $A_2BV_3F_{12}$ in addition to three $S = 1/2$ Ti^{3+} $A_2BTi_3F_{12}$. In order to reveal the effects of magnetic anisotropy and quantum fluctuation on the magnetism of KLAFs, it is important to compare crystal structure and magnetic properties of $S = 1$ $A_2BV_3F_{12}$ with those of $S = 1/2$ $A_2BTi_3F_{12}$. In the previous work, we investigated crystal structure and magnetic properties of $S = 1/2$ Ti^{3+} KLAFs $Cs_2KTi_3F_{12}$, $Cs_2NaTi_3F_{12}$, and $Rb_2NaTi_3F_{12}$ [23]. As well as $A_2BV_3F_{12}$, the distortion of framework of the kagome lattice becomes large with decreasing the ionic radii of A and B. In $A_2BTi_3F_{12}$, the distortion corresponds to the magnitude of anisotropy of M. Although all three compounds of $A_2BTi_3F_{12}$ have nearly the same antiferromagnetic interactions of $J \sim 45$ K and show no magnetic ordering, the magnetic behaviors at low temperatures and the ground states strongly depend on the distortion. As the distortion becomes large, anisotropy of M increases. Consequently, the ground state varies from a gapped disordered state ($Cs_2KTi_3F_{12}$) to a gapless disordered state ($Cs_2NaTi_3F_{12}$), and finally to a two components state having 1/3 nearly free spins ($Rb_2NaTi_3F_{12}$). Moreover, $Cs_2KTi_3F_{12}$ and $Cs_2NaTi_3F_{12}$ show 1/3 magnetization plateaulike behaviors irrespective of the direction of H.

By comparing the magnetic properties of $A_2BV_3F_{12}$ and $A_2BTi_3F_{12}$, we find three definite differences: the magnetic ground state, the relation between anisotropy of M and the distortion of framework of the kagome lattice, and the magnetization plateaus. As mentioned above, three $S = 1/2$ $A_2BTi_3F_{12}$ have disordered ground states, which strongly depend on the distortion of kagome lattices. In contrast, three $S = 1$ KLAFs $A_2BV_3F_{12}$ show magnetic ordering with distorted 120° structure or other nearly coplanar magnetic structure whose basal spin plane is perpendicular to the kagome plane. We think that possible origins of different ground states between $A_2BTi_3F_{12}$ and $A_2BV_3F_{12}$ are a distortion of kagome lattices, magnetic anisotropy, and decrease of quantum fluctuation. Although the distortion helps stabilization of magnetic ordering in $A_2BV_3F_{12}$, the distortion of $A_2BV_3F_{12}$ is smaller than that of $A_2BTi_3F_{12}$ with each combination of A and B. Thus magnetic ordering in $A_2BV_3F_{12}$ is mainly due to large Ising-like anisotropy and decrease of quantum fluctuation.

Contrary to $S = 1/2$ $A_2BTi_3F_{12}$, anisotropy of M does not correspond to the distortion of framework of the kagome lattice in $A_2BV_3F_{12}$, which becomes large with decreasing the ionic radii of A and B. Our experimental results reveal that anisotropy of M at low temperatures becomes larger in the order of $Cs_2NaV_3F_{12}$, $Cs_2KV_3F_{12}$, and $Rb_2NaV_3F_{12}$. The magnitude of Ising-like single ion anisotropy $|D|$ and difference of J_i are considered to cause the anisotropy of M. Larger $|D|$ enhances spin canting along the easy axis [16], since the basal spin plane includes the $\perp ab$ direction (easy axis). In addition, larger difference of J_i can be desirable to enhance spin canting [36,37]. Thus the M value for $H \perp ab$, which increases with increasing the magnitude of spin canting, becomes large with increasing $|D|$ and difference of J_i. In contrast, with increasing H for $H \parallel ab$, all V^{3+} spins incline gradually toward the H direction, forming an "umbrellalike" structure. Hence the M value for $H \parallel ab$ becomes small with increasing $|D|$. Consequently, as $|D|$ and the difference of J_i increase, anisotropy of M becomes large. Although the distortion of framework of $Cs_2KV_3F_{12}$ is the smallest among $A_2BV_3F_{12}$, anisotropy of $Cs_2KV_3F_{12}$ is larger than that of $Cs_2NaV_3F_{12}$. The fact suggests that $Cs_2KV_3F_{12}$ have larger $|D|$ and difference of J_i. $Cs_2KV_3F_{12}$ has lower symmetry of the crystal structure than $Cs_2NaV_3F_{12}$ and $Rb_2NaV_3F_{12}$, and five V^{3+} sites are present for $Cs_2KV_3F_{12}$ (three V^{3+} sites for $Cs_2NaV_3F_{12}$ and $Rb_2NaV_3F_{12}$). As a result, $|D|$ and difference of J_i of $Cs_2KV_3F_{12}$ are considered to be larger than those of $Cs_2NaV_3F_{12}$, which causes larger anisotropy of $Cs_2KV_3F_{12}$ than $Cs_2NaV_3F_{12}$.

Owing to $|D|$ and the difference of J_i, the magnetization plateaus observed in $A_2BV_3F_{12}$ are anisotropic and stabilized, which is remarkably different from the 1/3 magnetization plateaulike behaviors in $A_2BTi_3F_{12}$. The M-H curves of $A_2BV_3F_{12}$ for $H \perp ab$ show 1/3 and 2/3 magnetization plateaus, which become more distinct in the order of $Cs_2NaV_3F_{12}$, $Cs_2KV_3F_{12}$, and $Rb_2NaV_3F_{12}$. The result can be easily understood by the suggestion that $|D|$ and the difference of J_i become larger in this order. In addition, the 2/3 magnetization-plateau state can appear by the small

monoclinic distortion of kagome lattice. There are three spins in the unit cell of the ideal kagome lattice. In contrast, six spins are needed in the magnetic unit cell in order to realize the 2/3 magnetization plateau, and thus doubling of the unit cell is required. In $A_2BV_3F_{12}$, the crystal structure is monoclinic with $P2_1/m$ or $P2_1/c$, which gives six spins in the kagome plane of the unit cell. Therefore, the 2/3 magnetization-plateau state for $H \perp ab$ in $A_2BV_3F_{12}$ can be stabilized by the combination of the small monoclinic distortion of kagome lattice, spin frustration of kagome lattice, and Ising-like anisotropy.

No magnetization plateau for $H \parallel ab$ in $A_2BV_3F_{12}$ also can be understood by $|D|$ and decrease of quantum fluctuation. The 1/3 magnetization plateaulike behaviors in $Cs_2KTi_3F_{12}$ and $Cs_2NaTi_3F_{12}$ irrespective of the direction of H are considered to be caused by quantum fluctuation [23]. The quantum fluctuation of $A_2BV_3F_{12}$ is smaller than that of $S = 1/2$ $A_2BTi_3F_{12}$. If the 1/3 and 2/3 plateau states are present for $H \parallel ab$ in $A_2BV_3F_{12}$, spin arrangements are collinear which are perpendicular to the easy axis, and thus Ising-like single ion-anisotropy energy $DS^2_{\perp ab}$ is the highest. That is why no magnetization plateau is observed for $H \parallel ab$ in $A_2BV_3F_{12}$. In particular, jumps of M in the M-H curves of $Rb_2NaV_3F_{12}$ at $M/M_{sat} = 1/3$ for $H \parallel b$ and at $M/M_{sat} = 2/3$ for $H \parallel a$ are considered to be due to destabilization of the collinear spin states. It should be noted that two types of anomalies with hysteresis are independently observed for $H \parallel a$ and $H \parallel b$, and that three jumps of M are observed for $H \parallel a$. The situation cannot be explained by the simple Ising or XY kagome model. As mentioned above, in-plane anisotropy of M is observed. A spin-flop–like transition occurs at 1 T with hysteresis for $H \parallel b$. Thus the anomalies of M-H curves under high magnetization fields are considered to be due to coupling between in-plane magnetic anisotropy and destabilization of collinear spin structure perpendicular to the easy axis of Ising-like anisotropy.

Such anisotropic magnetization plateaus are observed in some TLAFs. For example, in $S = 7/2$ $GdPd_2Al_3$ with easy axis anisotropy, a 1/3 magnetization plateau appears when H is parallel to the easy axis, while no anomaly is observed under in-plane magnetic fields [28]. The magnetization plateaus in $A_2BV_3F_{12}$ are similar to that of $GdPd_2Al_3$, whereas M-H curves for $H \parallel ab$ in $A_2BV_3F_{12}$, particularly those in $Rb_2NaV_3F_{12}$, show destabilization of collinear spin structure. The destabilization is seemingly correlated with anomalies at $M/M_{sat} = 1/3$ in some TLAFs with easy plane anisotropy, such as $Ba_3CoSb_2O_9$ and $CsCuCl_3$, which have 120° structure in the triangular plane as the ground states. In these compounds, 1/3 magnetization plateaus appear under in-plane magnetic fields, whereas a cusp of M ($Ba_3CoSb_2O_9$ [30]) or a jump of M ($CsCuCl_3$ [38]) is observed at $M/M_{sat} = 1/3$ under out-plane fields. Under out-plane fields, a magnetic phase transition from "umbrellalike" structure to a 2:1 canted coplanar phase without the up-up-down state is considered to occur at $M/M_{sat} = 1/3$ owing to competition between quantum fluctuation and easy plane magnetic anisotropy [30,38,39]. In spite of the difference between easy axis and easy plane anisotropy and the difference between triangular and kagome lattices, similar magnetic phase transitions would occur in $Rb_2NaV_3F_{12}$ at $M/M_{sat} = 1/3$ for $H \parallel b$ and at $M/M_{sat} = 2/3$ for $H \parallel a$.

We also mention the effect of the DM interaction $D_{DM}(S_i \times S_j)$ in $A_2BV_3F_{12}$. Contrary to triangular magnets, kagome magnets have the DM interaction, since they have no inversion center at the middle point of neighboring magnetic ions. The large spin-orbit interaction in $A_2BV_3F_{12}$ induces relatively large magnitude of the DM interaction. In KLAFs, the DM interaction is known to stabilize the "$q = 0$" 120° structure whose spin plane includes the kagome plane [17]. In contrast, in $A_2BV_3F_{12}$, the basal spin plane is perpendicular to the kagome plane, suggesting that Ising-like anisotropy is dominant compared with the DM interaction. However, the DM interaction can also affect the magnetic state under high magnetic fields. Since collinear spin arrangements along the $\perp ab$ direction are realized in the 1/3 and 2/3 magnetization-plateau states, the DM interaction is considered to destabilize the plateau states by producing spin canting. That is why the slope of M-H in the plateau states is not zero but has finite values even in $Rb_2NaV_3F_{12}$.

As mentioned before, V^{3+} KLAFs $A_2BV_3F_{12}$ are categorized as KLAFs with Ising-like anisotropy, which is markedly different from almost isotropic $S = 1/2$ KLAFs $A_2BTi_3F_{12}$. There are few experimental studies of KLAFs with Ising-like anisotropy owing to absence of the suitable compounds. Our experimental results reveal that KLAFs $A_2BV_3F_{12}$ with Ising-like anisotropy exhibit various magnetic field induced phases including 1/3 and 2/3 magnetization plateaus. Thus KLAFs with Ising-like anisotropy give a good stage to search for magnetic field induced unconventional phenomena.

V. CONCLUSION

We discovered three $S = 1$ kagome lattice antiferromagnets $Cs_2KV_3F_{12}$ $Cs_2NaV_3F_{12}$, and $Rb_2NaV_3F_{12}$ with Ising-like anisotropy and succeeded in growing their single crystals. We also clarified the crystal structure and magnetic properties using single crystals. The distortion of framework of the kagome lattice becomes large with decreasing the ionic radii of A and B. However, while $Cs_2NaV_3F_{12}$ and $Rb_2NaV_3F_{12}$ crystallize in a monoclinic system of $P2_1/m$ as well as $A_2BTi_3F_{12}$, $Cs_2KV_3F_{12}$ possesses the lower symmetry of $P2_1/c$ with doubling of the unit cell along the c axis. As a result, anisotropy of M becomes large in the order of $Cs_2NaV_3F_{12}$, $Cs_2KV_3F_{12}$, and $Rb_2NaV_3F_{12}$. Three compounds form magnetic ordering with distorted 120° structure or other nearly coplanar magnetic structure whose basal spin plane is perpendicular to the kagome plane at low temperatures, which is mainly due to large Ising-like magnetic anisotropy and decrease of quantum fluctuation. The M-H curves for $H \perp ab$ show distinct 1/3 and 2/3 magnetization plateaus. These plateaus become more distinct in the order of the smallest anisotropy. In particular, the 2/3 magnetization plateaus are notable magnetic phenomena in kagome lattice antiferromagnets and are due to the combination of intrinsic spin frustration of kagome lattice, Ising-like single ion anisotropy, and the small distortion of kagome lattices. Moreover, jumps of M at $M/M_{sat} = 1/3$ and 2/3 are observed for $H \parallel ab$, which are likely due to coupling between destabilization of the plateaus, spin frustration, possible quantum fluctuation, and in-plane magnetic anisotropy.

ACKNOWLEDGMENTS

This work was supported by JSPS KAKENHI Grant No. 15J02000 and a Grant-in-Aid for Scientific Research (C) from the Japan Society for the Promotion of Science (Grant No. 24540345). The synchrotron radiation experiments at the Photon Factory were performed with the approval of the Photon Factory Program Advisory Committee (Proposal No. 2014S2-003).

[1] A. P. Ramirez, Annu. Rev. Mater. Sci. **24**, 453 (1994).
[2] C. Zeng and V. Elser, Phys. Rev. B **42**, 8436 (1990).
[3] N. Elstner and A. P. Young, Phys. Rev. B **50**, 6871 (1994).
[4] Ch. Waldtmann, H.-U. Everts, B. Bernu, C. Lhuillier, P. Sindzingre, P. Lecheminant, and L. Pierre, Eur. Phys. J. B **2**, 501 (1998).
[5] G. Misguich, D. Serban, and V. Pasquier, Phys. Rev. Lett. **89**, 137202 (2002).
[6] S. Yan, D. A. Huse, and S. R. White, Science **332**, 1173 (2011).
[7] Y. M. Lu, Y. Ran, and P. A. Lee, Phys. Rev. B **83**, 224413 (2011).
[8] S. Depenbrock, I. P. McCulloch, and U. Schollwöck, Phys. Rev. Lett. **109**, 067201 (2012).
[9] S. Ryu, O. I. Motrunich, J. Alicea, and M. P. A. Fisher, Phys. Rev. B **75**, 184406 (2007).
[10] Y. Ran, M. Hermele, P. A. Lee, and X. G. Wen, Phys. Rev. Lett. **98**, 117205 (2007).
[11] M. Hermele, Y. Ran, P. A. Lee, and X. G. Wen, Phys. Rev. B **77**, 224413 (2008).
[12] K. Hida, J. Phys. Soc. Jpn. **69**, 4003 (2000).
[13] S. Nishimoto and M. Nakamura, Phys. Rev. B **92**, 140412 (2015).
[14] H. Asakawa and M. Suzuki, Physica A **198**, 210 (1993).
[15] H. J. Changlani and A. M. Läuchli, Phys. Rev. B **91**, 100407 (2015).
[16] A. Kuroda and S. Miyashita, J. Phys. Soc. Jpn. **64**, 4509 (1995).
[17] O. Cépas, C. M. Fong, P. W. Leung, and C. Lhuillier, Phys. Rev. B **78**, 140405 (2008).
[18] M. Nishiyama, S. Maegawa, T. Inami, and Y. Oka, Phys. Rev. B **67**, 224435 (2003).
[19] K. Okuta, S. Hara H. Sato, Y. Narumi, and K. Kindo, J. Phys. Soc. Jpn. **80**, 063703 (2011).
[20] K. Hida, J. Phys. Soc. Jpn. **70**, 3673 (2001).
[21] S. Nishimoto, N. Shibata, and C. Hotta, Nat. Commun. **4**, 2287 (2013).
[22] T. Picot, M. Ziegler, R. Orús, and D. Poilblanc, Phys. Rev. B **93**, 060407 (2016).
[23] M. Goto, H. Ueda, C. Michioka, A. Matsuo, K. Kindo, and K. Yoshimura, Phys. Rev. B **94**, 104432 (2016).
[24] N. Wada, T. Kobayashi, H. Yano, T. Okuno, A. Yamaguchi, and K. Awaga, J. Phys. Soc. Jpn. **66**, 961 (1997).
[25] T. Matsushita, N. Hamaguchi, K. Shimizu, N. Wada, W. Fujita, K. Awaga, A. Yamaguchi, and H. Ishimoto, J. Phys. Soc. Jpn. **79**, 093701 (2010).
[26] S. Miyashita, J. Phys. Soc. Jpn. **55**, 3605 (1986).
[27] A. V. Chubukov and D. I. Golosov, J. Phys.: Condens. Matter **3**, 69 (1991).
[28] H. Kitazawa, H. Suzuki, H. Abe, J. Tang, and G. Kido, Physica B **259**, 890 (1999).
[29] L. E. Svistov, A. I. Smirnov, L. A. Prozorova, O. A. Petrenko, L. N. Demianets, and A. Ya. Shapiro, Phys. Rev. B **67**, 094434 (2003).
[30] T. Susuki, N. Kurita, T. Tanaka, H. Nojiri, A. Matsuo, K. Kindo, and H. Tanaka, Phys. Rev. Lett. **110**, 267201 (2013).
[31] G. M. Sheldrick, SHELXL-97, *Program for Structure Refinement*, University of Göttingen, Germany, 1997.
[32] D. Babel, Z. Anorg. Allg. Chem. **387**, 161 (1972).
[33] Z. Hiroi, M. Hanawa, N. Kobayashi, M. Nohara, H. Takagi, Y. Kato, and M. Takigawa, J. Phys. Soc. Jpn. **70**, 3377 (2001).
[34] M. Yoshida, Y. Okamoto, M. Takigawa, and Z. Hiroi, J. Phys. Soc. Jpn. **82**, 013702 (2013).
[35] B. N. Figgis, *Introduction to Ligand Fields* (Interscience, New York, 1966).
[36] T. Yavors'kii, W. Apel, and H.-U. Everts, Phys. Rev. B **76**, 064430 (2007).
[37] P. H. Y. Li, R. F. Bishop, C. E. Campbell, D. J. J. Farnell, O. Götze, and J. Richter, Phys. Rev. B **86**, 214403 (2012).
[38] M. Motokawa, M. Arai, H. Ohta, M. Mino, H. Tanaka, and K. Ubukata, Physica B **211**, 199 (1995).
[39] T. Nikuni and H. Shiba, J. Phys. Soc. Jpn. **62**, 3268 (1993).